Structural, Swanepoel's method, optical and electrical parameters of vacuum evaporated $Zn_{50}Se_{50}$ thin films

A. B. Alwany[a,b,*], G. M. Youssef[b], M. A. Algradee[a], M. A. Abdel-Rahim[c], A. Alnakhlani[a,d], B. Hassan[a,d]
[a]*Physics Department. Faculty of Science, Ibb University. Ibb, Yemen*
[b]*Laboratory of Materials Sciences and Solar Cells, Physics Department, Faculty of Science, Ain Shams University, Abbasia, Cairo, Egypt*
[c]*Physics Department. Faculty of Science, Assuit University. Assuit, Egypt*
[d]*Physics Department, College of Science and Arts, Qassim University, Al-Asyah, Saudi Arabia*

Thin films of $Zn_{50}Se_{50}$ were prepared by the vacuum evaporation technique on glass substrates. The influence of annealing temperature ($T_{ann.}$) on the structural and optical properties of *ZnSe* polycrystalline films was investigated using X-ray diffraction (*XRD*), scanning electron microscopy (*SEM*) and optical transmittance T (λ). The crystalline phases that were found in the $Zn_{50}Se_{50}$ thin films are ZnSe, Se and Zn. The refractive index (n) and the thickness of the films (d) were calculated using Swanepoel's method for the films annealed at (*423 K*). The mechanism of optical absorption follows the rule of direct transition. The values of band gap (E_G) were found to decrease from about *2.933* to *2.635 eV* with the increasin of the $T_{ann.}$ from *300* to *423 K*. Urbach energy (E_U) was calculated and found to the increase by increasing T_{ann}. The dispersion of the n was discussed in terms of the single-oscillator Wemple and DiDomenico model. The Arrhenius formula was used to discuss the electrical conductivity (σ_{DC}), activation energy (ΔE) and pre-exponential factor (σ_o).

(Received October 14, 2022; Accepted January 4, 2023)

Keywords: Chalcogenide glasses, thin films, annealing temperature, Swanepoel's method, optical and electrical properties

1. Introduction

Binary glass (*Zn-Se*) has gained much attention due to its low resistivity and wide-optical band gap (E_G). The E_G of *II-VI* semiconductor extends from *2.7* to *2.9 eV* at room temperature (RT) [1-7]. Since *Zn-Se* has a wide E_G, its non-toxicity and its ability to provide a better lattice match with *Cu*(*In*, *Ga*)Se_2 (*CIGS*) absorber, therefore Zn-Se is used as a buffer layer material instead of *CdS* in (*CIGS*) based solar cells. Also *Zn-Se*/*Si* hetrojunction is of specific interest since this structure provides effective solar cells with on efficiency of 17.5 % [8-10]. Furthermore, *Zn-Se* is used as a window layer for the fabrication of thin films, solar cells, laser screens, laser diodes, thin films transistors and blue green light emitting diodes [11-13].

Zn-Se has been studied by many researchers as amorphous or crystalline as well as thin films to investigate its optical, electrical, and structural properties [1, 6, 14, 15]. On the other hand, the effect of defects on the degradation of *ZnSe*-based white *LEDs* has been investigated, and the n-*ZnSe*/*p-GaAs* heterojunctions offer a large photo-voltaic effect [16, 17]. Because of these good and unique properties, there are many different growth techniques used to prepare Zn-Se films, for example atomic layer epitaxy (*ALE*), molecular beam epitaxy (*MBE*), organo-metallic chemical vapor deposition (*OMCVD*), thermal evaporation under vacuum, solution growth spray pyrolysis etc. [18-22]. In this study, the vacuum evaporation technique was used to prepare *ZnSe* thin films due to its simplicity; low cost reproducibility, and this technique is suitable for producing high-

*Corresponding author: abdualwhab@yahoo.com
https://doi.org/10.15251/CL.2023.201.19

quality films [23, 24]. To the best of our knowledge, detailed studies on optical properties by Swanepoel's method are looking.

In the present paper, we report the composition, structural, optical, and electrical properties of vacuum evaporated $Zn_{50}Se_{50}$ thin films. The *d* and *n* were evaluated from Swanepoel's method. Different techniques such as (EDAX), (XRD), (SEM), and spectrophotometer are used to achieve the aim of this work.

2. Experimental details

The bulk glassy material was prepared by using the well-known melt quenching method, in which highly pure *Zn* and *Se* elements (99.999%) were alloyed to obtain $Zn_{50}Se_{50}$. These constituents were weighted in accordance with their atomic percentages by using a sensitive electronic balance with an accuracy of *0.1* mg. The weighted elements were placed into a quartz glass ampoule and sealed under a vacuum of 10^{-5} Torr. The sealed ampoule was heated in a Heraus programmable tube furnace (type *R 07115*); the heating rate was approximately *3.5 K/min*. The temperature was kept at *1150 K* for *24* hours. The ampoule was manually stirred for realizing the homogeneity of the composition. After that, the ampoule was quenched into ice-cooled water. Thin films were prepared by thermal evaporation under vacuum of 10^{-5} Torr using the Edwards *E-306* coating system. A constant evaporation rate (*6 nm/sec*) was used to deposit the films. The evaporation rates as well as the films thickness were controlled using a quartz crystal monitor (*FTM5*), where the *d* of the film was *940 nm*. The film composition was checked using the (*EDAX*) technique. $Zn_{50}Se_{50}$ films were annealed at different temperature ($300 \leq T_{ann.} \leq 423$ *K*) for one hour under N-gas. The morphology for as-deposited and annealed films was investigated using (*SEM*) type *JEOLJSM-T200*. The crystalline phases of the films were identified using a Philips diffractometer type *1710* with $\lambda = 1.5416$ *Å*. The optical transmittance $T(\lambda)$ of the as-deposited and annealed $Zn_{50}Se_{50}$ films was measured at RT using a double-beam spectrophotometer (*SHIMADZU UV-2101* combined with a *PC*) in the wavelength, (*300–900 nm)*. The electrical measurements were carried out for as-deposited and different annealed films. Of a conventional circuit involving a keithley 610C electrometer was used. The electrical measurements were carried out during the heating of the thin films from RT to 433 K under a constant flow N-gas, and cooling down to RT.

3. Results and discussion

3.1. Structure

The EDAX was used to investigate the composition of $Zn_{50}Se_{50}$ thin films. As observed from Fig. 1, only peaks corresponding to *Zn* and *Se* were found, and the ratios of the atomic percentages of *Zn* and Se were found to be *47.68* and *52.32*, respectively.

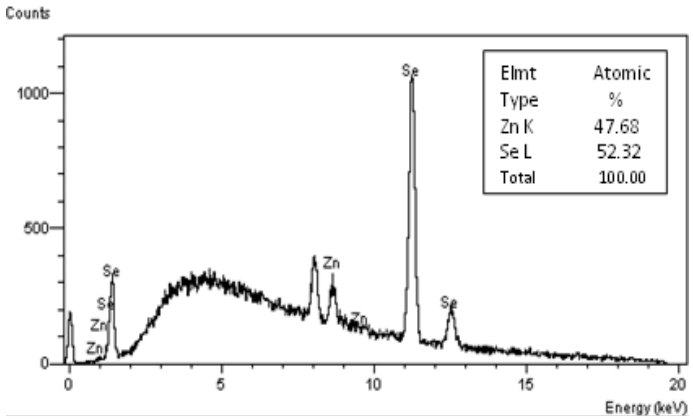

Fig. 1. EDX spectrum of as-deposited $Zn_{50}Se_{50}$ thin films.

The image of the *SEM* of the as-deposited and annealed at *423 K* for *1 h ZnSe* thin films is shown in Fig. 2(a and b).

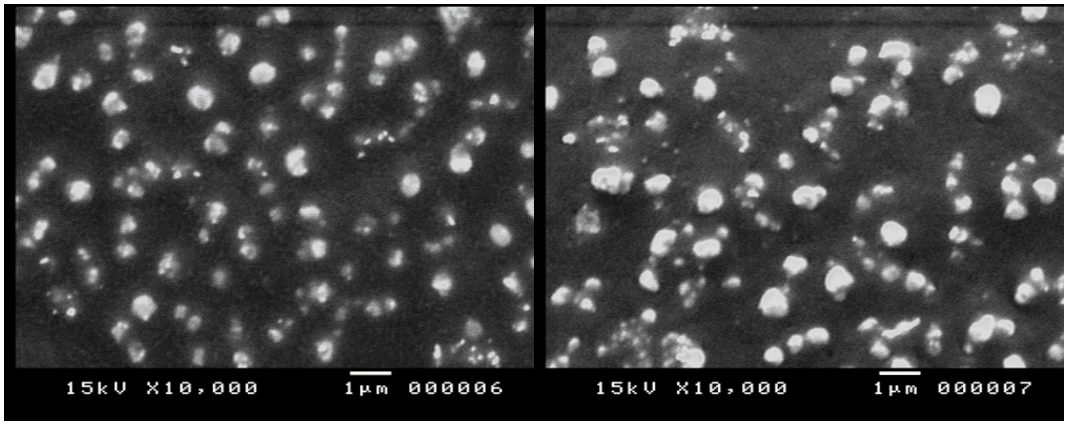

(a) *(b)*

Fig. 2. The SEM photograph for $Zn_{50}Se_{50}$ thin films (a) as-deposited and (b) annealed at 423 K for 1h.

The image depicted in Fig. 2(a), illustrates that the crystalline phase is embedded in an amorphous matrix, and small nanosized grains were distributed over a large area of the film. On the other hand, the crystalline size of *ZnSe* thin films is improved after $T_{ann.}$ at *423 K* for *1 h* as shown in Fig. 2 (b). Generally, it is found that the nanoparticles (NPs) size increases after sample annealing due to the effective agglomeration of smaller NPs into larger NPs.

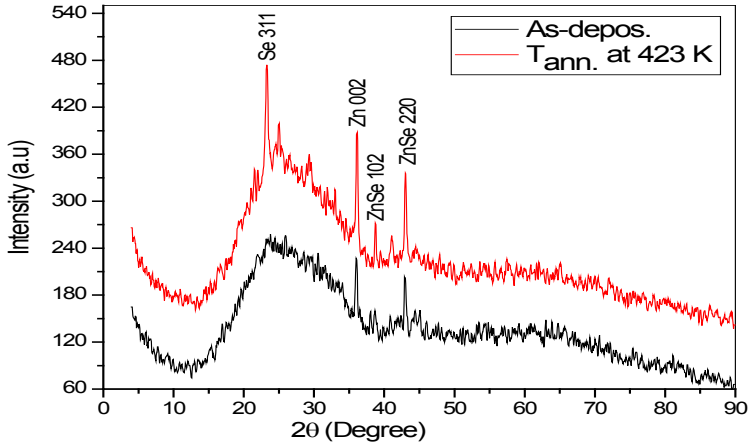

Fig. 3. The XRD patterns of $Zn_{50}Se_{50}$ thin films for as-deposited and annealed at 423 K for 1 h.

The XRD spectra of $Zn_{50}Se_{50}$ thin films for as-deposited and annealed at *423 K* for *1 h* are depicted in Fig. (3). The layers showed peaks at $2\theta \approx 38.109^{o}$ and $2\theta \approx 43.389^{o}$ correspond to the (*102*) and (*220*) reflections of $Zn_{50}Se_{50}$ phase respectively, which are polycrystalline, and have a f.c.c cubic zinc blende structure. Similar phases observed with annealing temperature by M.A. Abdel-Rahim et al. [1] and M. Husain et al. [25]. Also there are two phases are found as shown in Fig.(3). The *Zn*-phase at $2\theta \approx 36.090^{o}$ is reflected from the crystallographic plane (*002*) and, the *Se*-phase at $2\theta \approx 23.242^{o}$ which appeared after $T_{ann.}$ and corresponds to the crystallographic plane (*311*).

The lattice constant (a) for the cubic phase structure is obtained from the XRD analysis using the following relationship,

$$a = \frac{\lambda(h^2+k^2+l^2)^{1/2}}{2sin\theta} \quad (1)$$

where *h, k, l* are the miller indices, θ is the diffraction spectra (Bragg's angle) and λ, (*1.5416 Å*) is the wavelength of the XRD used. Lattice constant 'a' for as-deposited *ZnSe* thin films and annealed at 423 K is observed in Table (1). It is observed that the change in lattice constant (a) for the as-deposited and annealed thin film over the bulk clearly suggests that the film grains are strained, which may be due to the nature and concentration of the native imperfections changing.

The average of particle size (P) of $Zn_{50}Se_{50}$ phase was calculated using Scherer's equation [6, 26],

$$P = \frac{0.94\,\lambda}{Wcos\theta} \quad (2)$$

where, W is the full width at half maximum intensity (*FWHM*), and θ is the angle between the incident and the scattered XRD.

The value of lattice strain (ε) for *ZnSe* thin films was calculated using this relation,

$$\varepsilon = (\frac{\lambda}{Pcos\theta} - W) \times \frac{1}{tan\theta} \quad (3)$$

The value of dislocation density (δ) is defined as the length of dislocation lines per unit volume of the particle and is given by,

$$\delta = \frac{1}{P^2} \quad (4)$$

The average values of the above parameters (P, ε, δ) are summarized in Table (1). It is observed that the average of P increases with the increasing T_{ann}, while the average ε of the *ZnSe* phase decreases with the increasing $T_{ann.}$ as can be seen from Table (1). In addition to that, the δ is found to decreases with the increasing of the $T_{ann.}$ indicating to improvement in crystallinity, where the improvement in crystallinity is due to sintering of nanocrystals into effectively large crystal after $T_{ann.}$ of the films. This result is in good agreement with the previous work [27-29].

Table. 1. Structure parameters of $Zn_{50}Se_{50}$ thin films for as-deposited and annealed at 423 K for 1h.

$Zn_{50}Se_{50}$	d_{stand} [Å]	d_{exp} [Å]	2θ [Deg.]	h k l	a [Å]	Kind of phase	P [nm]	Average of p [nm]	Average of ε [$lin^{-2}.m^{-4}$]	Average of $\delta \times 10^{15}$ [$lines/m^2$]
As-deposited	2.386 2.0046	2.359 2.0754	38.109 43.578	102 220	5.279 5.873	ZnSe ZnSe	*79.522* 57.853	68.687	0.0594	0.2119
T_{ann} at 423 [K]	2.386 2.0046	2.356 2.0702	38.234 43.819	102 220	5.263 5.842	ZnSe ZnSe	99.451 62.300	80.875	0.0505	0.1528

3.2. Optical properties

In this part of the paper, the optical properties of $Zn_{50}Se_{50}$ thin films for as-deposited and different annealed temperature (*323, 373,* and *423 K*) for *1 h* were studied using $T(\lambda)$ in the λ range from 300 to 900 nm.

The recorded of $T(\lambda)$ spectra for the as-deposited and different annealed $Zn_{50}Se_{50}$ thin films are presented in Fig. (4). One can observe that, the appearance of interference fringes phenomena occurred in the films. On the other hand, this phenomenon confirms the formation of smooth and

uniform films, also indicates the crystallinity of the films [30]. The *n* and *d* of the film were calculated from the typical $T(\lambda)$ spectrogram of the film annealed at *423 K*, as shown in Fig. (5) using Swanepall's method [31]. The spectrum of $T(\lambda)$ can nearly be divided into four regions (*i*) transparent region, where the absorption coefficient (α) = *0* (*ii*) weak absorption region, the α at this region is small, whereas the $T(\lambda)$ start to reduced (*iii*) medium absorption region, the α will be large, therefor the $T(\lambda)$ decreases (*iv*) strong absorption region, where the $T(\lambda)$ decreases significantly due to the effect of α, (Fig. 4 shows these four regions).

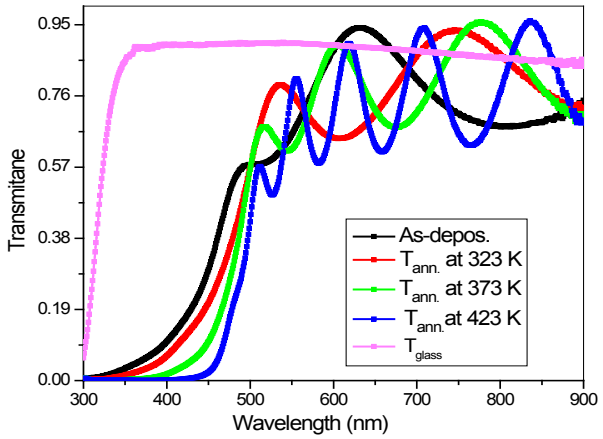

Fig. 4. T(λ) behavior for as-deposited and annealed $Zn_{50}Se_{50}$ thin films.

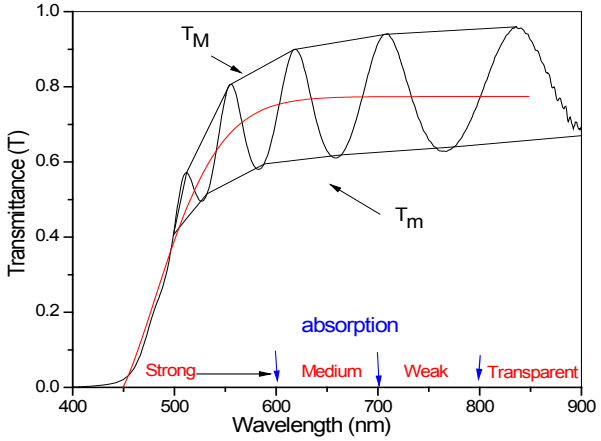

Fig. 5. T(λ) annealed at 423 K for 1h $Zn_{50}Se_{50}$ thin films, including the maximum (T_M) and minimum (T_m) transmittance envelope curves.

Fig. (5) shows the envelopes around the interference maximum and minimum of the transmittance film annealed at *423 K* for *1 h*. The *n* values of the film were calculated using the following equation [31],

$$n = \left[N + (N^2 - n_s)^{1/2}\right]^{1/2} \tag{5}$$

where n_s is the refractive index of the substrate alone, and *N* is the parameter given by,

$$N = 2n_s \times \left(\frac{T_M - T_m}{T_M T_m}\right) + \frac{n_s^2 + 1}{2} \tag{6}$$

T_M and T_m indicate the transmission maximum and corresponding minimum at the same λ. On the other hand, the n_s is given by this relation [31, 32],

$$n_s = \frac{1}{T_s} + \left(\frac{1}{T_s^2} - 1\right)^{1/2} \quad (7)$$

T_s, is the transmittance of the glass substrate (in the absence of film), where its value was around 90.6 %, as the observed from the Fig. (4), and the value of n_s in this work equals 1.57. The basic equation for the interference fringe is given by,

$$2nd = m\lambda \quad (8)$$

where the order number m represents an integer or half integer for constructive and destructive interference, respectively.

Table 2. Values of λ, T_M, T_m,, n and d for transmittance annealed at 423 K for 1h $Zn_{50}Se_{50}$ thin films.

λ [nm]	T_M	T_m	n	d [nm]	m
838	0.969	0.640	2.462	890.720	5
765	0.946	0.629	2.464	910.328	5.5
705	0.939	0.625	2.467	937.589	6
657	0.916	0.612	2.477	973.577	6.5
614	0.902	0.606	2.476	1080.171	7
578	0.848	0.581	2.476	1042.264	7.5
551	0.816	0.566	2.476	~~1335.247~~	8
520	0.647	0.479	2.477		8.5
508	0.563	0.432	2.473		9

Table 2 shows the values of (n) which calculated from equation (*5*) and the values at the extremes of the spectrum T_M and T_m at different λ obtained from figure (4), also the values of (d) are shown in Table (2). Where the values of (d) have some dispersion, but the dispersion of the last value is large and it is rejected, this large dispersion which are due to (n) and (λ) is not accurate enough.

The absorption coefficient (α) of $Zn_{50}Se_{50}$ thin film for as-deposited and different annealed was computed using the experimental data of $T(\lambda)$ and $R(\lambda)$ according to the following relation [6],

$$\propto = \frac{1}{d}\ln\left(\frac{(1-R)^2}{T}\right) \quad (9)$$

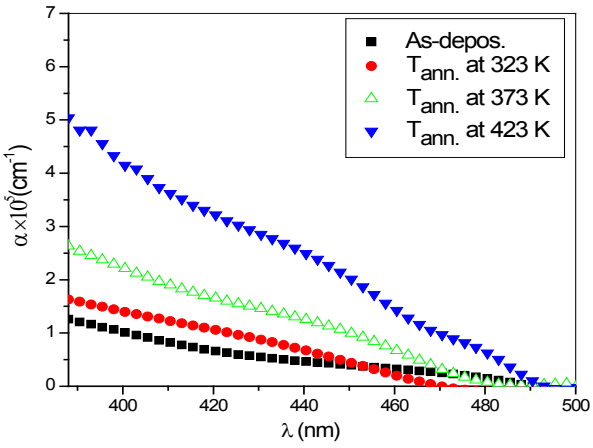

Fig. 6. The α for the as-deposited and annealed $Zn_{50}Se_{50}$ thin films.

It is observed from Fig. 6 that, the (α) decreases with increasing λ, and is affected by the annealing temperature. The annealed film at a higher temperature gives a higher absorption. It is clear that the increase in the absorption coefficient with increasing annealing temperature is due to the increase in the size of the crystals, where the intercrystallite boundaries contain impurities and structural defects. On the other hand, the intercrystallite boundaries, being highly disordered and a sink for impurities, can have properties very different from those of the crystallites, giving a marked contribution to the absorption process in the thin films [30, 33].

The values of (E_G) for as-deposited and annealed films were determined by analyzing the optical data with the expression for the α, and the photon energy (E), [1] using the relation,

$$(\alpha E) = A\,(E - E_G)^r \tag{10}$$

where r is a number that determines the type of the optical transition (r =1/2 for allowed direct transitions, and r = 2 for allowed indirect transitions) and A is a constant that depends on the electron transition probability. The values of E_G calculated from the intersection of the straight lines in Fig. 7 with the x-axis at $(\alpha E)^2 = 0$ versus E for the direct E_G. These values of E_G listed in Table (3), it is clear that the E_G lie in the range, from *2.933* to *2.635 eV*, this result is in good agreement with the previous work [8]. The values of E_G were found to decreases with the increasing of $T_{ann.}$, this behavior is likely to be due to decreases in ε values and increase of P that was confirmed by our XRD measurements, [8, 13, 21]. On the other hand, the lattice expansion contributes to the decreased of E_G with the increase of the annealing temperature.

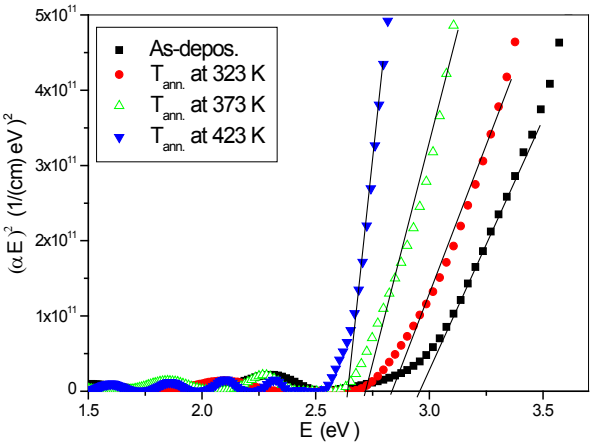

Fig. 7. Plot of $(\alpha E)^2$ vs. E for the as-deposited and annealed $Zn_{50}Se_{50}$ thin films.

Table 3. The E_G, E_e, E_o and E_d for the as-deposited and annealed $Zn_{50}Se_{50}$ thin films.

$T_{ann.}$ [K]	E_G [eV]	E_U [eV]	E_o [eV]	E_d [eV]
As-deposited	2.933	0.073	7.278	83.919
323	2.832	0.078	10.241	90.408
373	2.714	0.081	7.074	97.484
423	2.635	0.088	5.477	65.205

In the low absorption regions where the α laying between 10^2 and 10^4 cm^{-1}, are defined as Urbach's exponential tails region [34, 35], and it is given by the following equation.

$$ln(\alpha) = ln(\alpha_o) + E/E_U \tag{11}$$

where E is the photon energy and α_o is a constant. Therefore, plotting the dependence of $ln(\alpha)$ versus E as shown in Fig. (8) should give a straight line. The inverse of the slope gives E_U, and its values are shown in Table (3). It can be noted that, the (E_U) increases continuously with the increasing $T_{ann.}$, where E_U is a measure of the degree of disorder and structural defects such as dangling or broken bonds, as well as vacancies in the studied sample [36]. It was noted that, the increases in T_{ann} cause an increase in the E_U, thereby reducing the (E_G), as shown in Fig. (9).

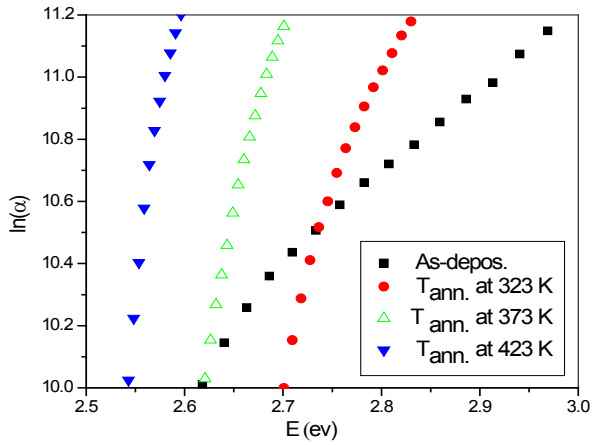

Fig. 8. Plot of ln(α) vs. E for as-deposited and annealed $Zn_{50}Se_{50}$ thin films.

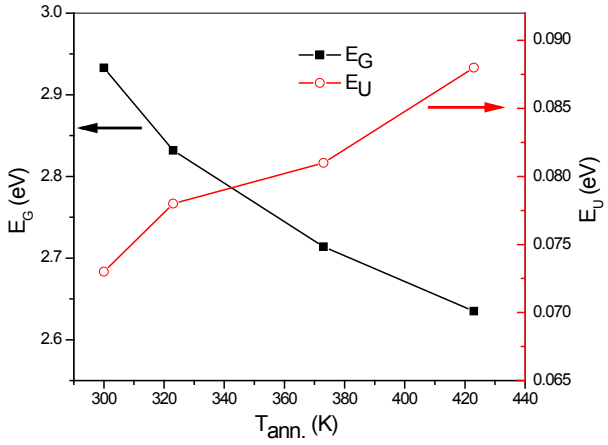

Fig. 9. Plot of E_G and E_U vs. $T_{ann.}$ for as-deposited and annealed $Zn_{50}Se_{50}$ thin films.

In the region of strong absorption the refractive index (n) was estimated from the data of the reflectivity (R) using the following equation [37],

$$n = \frac{1+\sqrt{R}}{1-\sqrt{R}} \tag{12}$$

Figure 10 shows the variance in refractive index (n) measured from the interference pattern at different annealing temperatures. It is noted that the refractive index increases with increasing wavelength to the peak observed at low wavelengths, in addition to the appearance of abnormal behavior in the refractive index, while dispersion is observed at high wavelengths.

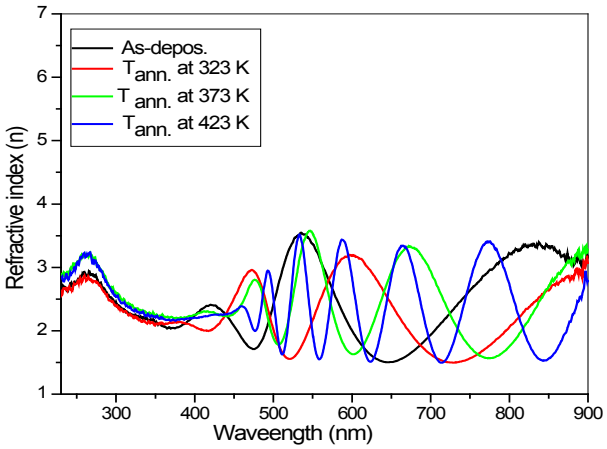

Fig. 10. Refractive index (n) versus wavelength (λ) of the as-deposited and annealed $Zn_{50}Se_{50}$ thin films.

The dispersion spectrum dependence of the refractive index was evaluated according to the single oscillator model proposed by Wemplle and DiDomennico (W.D), [38]. Where the W.D studied dispersion data for more than a hundred different materials. They conclude that all the optical data of crystalline and amorphous materials, as well as covalent and ionic materials could be described by the following equation,

$$(n^2 - 1)^{-1} = \frac{E_o}{E_d} - \frac{(E)^2}{E_0 E_d} \tag{13}$$

where E, is the incident photon energy, E_o is the single oscillator energy related to an average E_G, and E_d is the dispersion energy which measures the average strength of the interband optical transitions. In this relation, the dispersion was considered by electronic transitions. By plotting $(n^2 -1)^{-1}$ versus $(E)^2$ and fitting straight line E_o and E_d can be identified directly from the intercept and the slope as shown in Fig. 11. It can be observed that the equation (12) could be suitable for the description of the dispersion of n, where the values of (E_o and E_d) are shown in Table 3. It is found that, the values of E_o decrease while the values of E_d increase as the $T_{ann.}$ increases. The increasing of $T_{ann.}$ leads to the increasing of the atoms diffusion rate in the thin films, which gives more number of atoms at sites, where these atoms play an effective role in increasing the scattering centers of charge carriers and leads to the increas of E_d and decreas of E_o [39, 40].

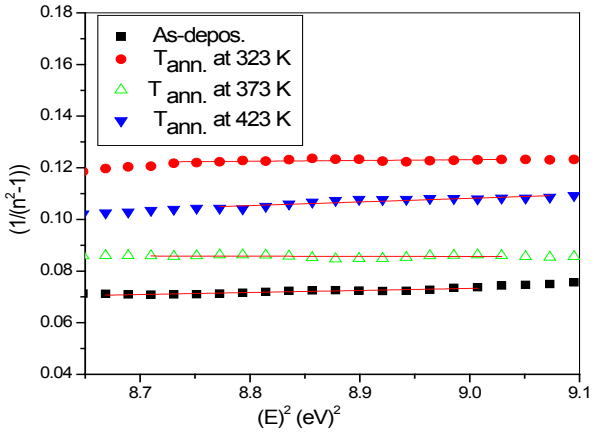

Fig. 11. Plots of $(n^2-1)^{-1}$ versus $(E)^2$ for the as-deposited and annealed $Zn_{50}Se_{50}$ thin films.

3.3. Electrical proprties

The effect of $T_{ann.}$ for 1 h on the electrical conductivity (σ_{DC}) of $Zn_{50}Se_{50}$ thin films was studied. Evaporated gap of Au electrodes were used on the thin films during electrical measurements. The temperature dependence on the σ_{DC} can be given by the Arrhenius formula [41],

$$\sigma_{DC} = \sigma_o e^{(-\frac{\Delta E}{k_B T})} \tag{14}$$

where ΔE denotes the activation energy for conduction, k_B, T are Boltzmann's constant and the sample absolute temperature, respectively, and σ_o is the pre-exponential factor, related to the mobility of charge carriers and the density of states.

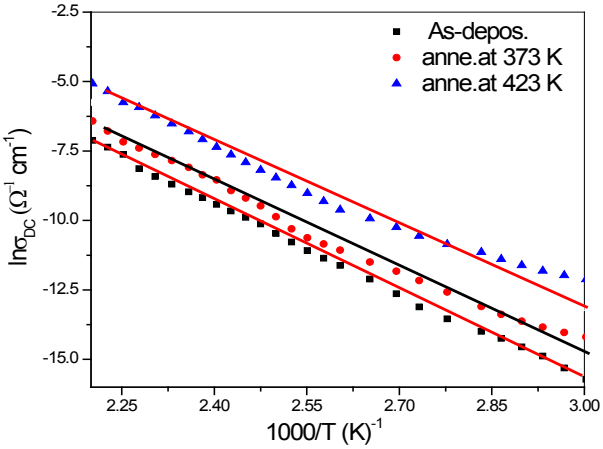

Fig. 12. $ln(\sigma_{DC})$ vs. 1000/T for the as-deposited and annealed $Zn_{50}Se_{50}$ thin films.

The relation between $ln(\sigma_{DC})$ and the reciprocal of temperature is given in Fig. 12. It is shown that the dark conductivity σ_{DC} increases with the increasing of the $T_{ann.}$. The ΔE for conduction and the σ_o were calculated from the slope of the straight line and from the intercept of the straight line with $ln(\sigma)$ axis respectively, and recorded in Table 4. In addition, the behavior of ΔE and σ_o versus $T_{ann.}$ is also shown in Fig. 13. It is clear from Table 4 and Fig. 13, that the values of both ΔE and σ_o decrease with the increase of the $T_{ann.}$. The decrease in the ΔE of conduction after the annealing temperature can be attributed to the improvement of the crystalline phase as discussed in the previous section, [42], also the decrease of the σ_o with the increasing of annealing temperature gives an indication on the number of localized in the gap. The decrease of σ_o marks the increase of localized states in the gap (discussed in the previous section) and vice versa.

Table 4. Values of ΔE (eV) and σ_o ($\Omega^{-1}cm^{-1}$), for as-prepared and annealed $Zn_{50}Se_{50}$ thin films.

$Zn_{50}Se_{50}$	ΔE [eV]	σ_o $[\Omega^{-1}cm^{-1}] \times 10^6$
As-prepared	*0.952*	*7.324*
373 [K]	*0.891*	*4.531*
423 [K]	*0.802*	*1.753*

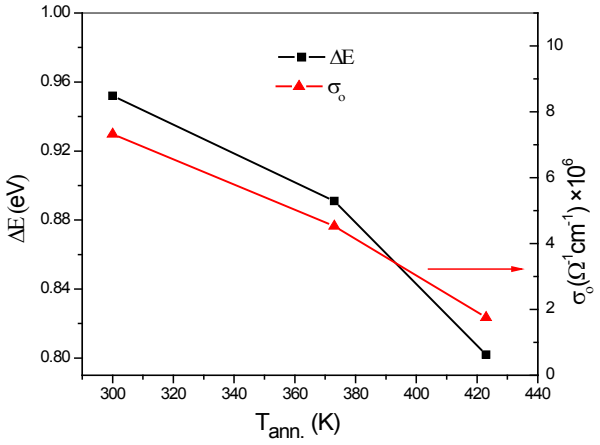

Fig. 13. Plots of ΔE and σ_o vs. $T_{ann.}$ for the as-deposited and different annealed $Zn_{50}Se_{50}$ thin films.

4. Conclusions

$Zn_{50}Se_{50}$ thin film has been prepared by using the thermal evaporation technique. The morphology of the samples was examined using *SEM*, where the as-deposited films and those annealed have a crystalline nature. The average particle size was found to increase by increasing $T_{ann.}$ as that have been observed from the XRD analyses. The Swanepole method was used to evaluate the n and d of thin films annealed at *423 K* for *1h*. In addition, the application of the Swanepoel method is straightforward, provided that the refractive index of the substrate (n_s) and the transmittance envelope curves (T_M) and (T_m) have been determined from transmittance data. For the as-deposited and annealed $Zn_{50}Se_{50}$ thin films direct allowed transition was observed and the E_G was decreased from *2.93 eV* to *2.63 eV* when the $T_{ann.}$ increased to *423 K*. The parameters E_o and E_d were evaluated and discussed by using Wemple-DiDmennco model. The dark conductivity σ_{DC} increases with the increasing of the T_{ann} and the ΔE for conduction and the σ_o decreased with the increasing T_{ann}.

Acknowledgments

This work was supported by Ibb University, Yemen, Ain-Shams University, Cairo, Egypt and Assuit University, Egypt.

References

[1] M. A. Abdel-Rahim, M. M. Hafiz, A. Elwhab. B. Alwany, Opt. Laser Technol. 47, (2013) 88; https://doi.org/10.1016/j.optlastec.2012.06.044

[2] M. Nasir, M. Zulfequar, Open J. Inorg. Non Met. Mater. 2(2), (2012); 11; https://doi.org/10.4236/ojinm.2012.22002

[3] M. F. Gromboni, T. C. Kastein, R. Matos, L. H. Mascaro, ECS Trans. 43(1), (2012) 211; https://doi.org/10.1149/1.4704960

[4] R. K. Kremer, M. Cardona, R. Lauck, G. Siegle, A.H. Romero, Phys. Rev. B 85(3), 035208 (2012); https://doi.org/10.1103/PhysRevB.85.035208

[5] Dohare, N. Mehta, Appl. Phys. A 114(2), (2014) 597; https://doi.org/10.1007/s00339-013-7624-4

[6] M.A. Abdel-Rahim, M.M. Hafiz, A. Elwhab.B. Alwany, Opt. Laser Technol. 44(4), (2012) 1116; https://doi.org/10.1016/j.optlastec.2011.10.003

[7] M. Nasir, M. A. M. Khan, M. Husain, M. Zulfequar, Mater. Sci. Appl. 2(05), (2011) 289; https://doi.org/10.4236/msa.2011.25038

[8] A. R. Balu, V. S. Nagarethinam, M. G. Syed Basheer Ahamed A. Thayumanavan. K. R. Murali, C. Sanjeeviraja, V. Swaminathan, M. Jayachandran. Mat. Sci. and Engineering B171 (2010) 93; https://doi.org/10.1016/j.mseb.2010.03.079

[9] M. Ganchev. N. Strahieva. E. Tsvetkova. I. Gadjov. J. Mater Sci.: Mater. Electron. 14 (2003) 847; https://doi.org/10.1023/A:1026154615666

[10] S. Venkatachalam, D. Mangalaraj, Sa.K. Narayandass, S. Velumani, P. Schabes-Retchkimanc, J. A. Ascencio. Mat. Chem. and Phys. 103 (2007) 305; https://doi.org/10.1016/j.matchemphys.2007.02.077

[11] A. G. Fisher, R. J. Paff, J. Phys. Chem. Solids 23 (1978) 218.

[12] L. Yan. J. A. Woollam. E. Franke. J. Vac. Sci. Technol. A 20 (3) (2002) 693; https://doi.org/10.1116/1.1463085

[13] R. B. Kale, C. D. Lokhande. R. S. Mane, Sung-Hwan Han. Appl. Surface Sci. 252 (2006) 5768; https://doi.org/10.1016/j.apsusc.2005.07.063

[14] G.I. Rusu, M.E. Popa, G.G. Rusu, Iulia Salaoru. Appl. Surface Sci. 218 (2003) 222; https://doi.org/10.1016/S0169-4332(03)00618-4

[15] M. A. Abdel-Rahim, M. M. Hafiz, A. Y. Abdel-Latief, Alaa M. Abd-Elnaiem, A. Elwhab. B. Alwany. Appl. Phys. A 119 (2015) 881; https://doi.org/10.1007/s00339-015-9031-5

[16] Tsuguru Shirakawa, Mat. Sci. and Engineering B91-92 (2002) 470; https://doi.org/10.1016/S0921-5107(01)01006-6

[17] O. de Melo, G. Santana, M. Melendez-Lira, I. Hernandez-Calderon, J. of Cryst. Growth 201/202 (1999) 971; https://doi.org/10.1016/S0022-0248(98)01502-4

[18] C. D. Lee.S. L. Min. S. K. Chang. J. Cryst. Growth 159 (1996) 108; https://doi.org/10.1016/0022-0248(95)00830-6

[19] J. S. Song. J. H. Chang. D. c. Oh. J. J. Kim. M. W. Cho. H. Makino. J. Cryst. Growth 249 (2003) 128; https://doi.org/10.1016/S0022-0248(02)02129-2

[20] K. Morimoto. J. Appl. Phys. 66 (1989) 4206; https://doi.org/10.1063/1.343959

[21] S. Venkatachalam. D. Mangalaraj. Sa. K. Narayandass. K. Kim. J. Yi. Phys. B. 358. (2005) 27; https://doi.org/10.1016/j.physb.2004.12.022

[22] M. Bedir. M. Oztas. O. F. Bakkaloglu. R. Ormanci. Eur. Phys. J. B. 45 (2005) 465; https://doi.org/10.1140/epjb/e2005-00207-3

[23] Khan SA, Zulfequar M, Husain M. Sol. State Communications 123 (2003) 463; https://doi.org/10.1016/S0038-1098(02)00147-3

[24] Prabakar K, Venkatachalamm S, Jeyachandran YL. Solar Energy Mat. and Solar Cells 81 (2004) 1; https://doi.org/10.1016/j.solmat.2003.08.008

[25] M. Husain, Beer Pal Singh, Sushil Kumar, T. P. Sharma, P.J. Sebastian. Solar Energy Mat. & Solar Cells 76 (2003) 399; https://doi.org/10.1016/S0927-0248(02)00291-X

[26] Venkatachalam S, Mangaloraj D, Narayandass SaK, Kim K, Yi. J. Phys. B 358 (2005) 27; https://doi.org/10.1016/j.physb.2004.12.022

[27] P. K. R. Kalita.B. K. Sharma. D. I. Das.Bull. Mater. Sci. 23 (2000), 313; https://doi.org/10.1007/BF02720089

[28] Ashraf M, Akhtar SMJ, Khan AF, Ali Z, Qayyum A. J. of alloys and comp. 509 (2011) 2414; https://doi.org/10.1016/j.jallcom.2010.11.032

[29] Venkatachalam S, Mangaloraj D, Narayandass SaK. Phys. B 393 (2007) 47; https://doi.org/10.1016/j.physb.2006.12.047

[30] N.Tigau, V. Ciupina, G. Prodan. J. of Cryst. Growth 277 (2005) 529; https://doi.org/10.1016/j.jcrysgro.2005.01.056

[31] R, Swanepole, J. Phps. E: Sci. Instrum. Vol. 16, (1983) 1214; https://doi.org/10.1088/0022-3735/16/12/023

[32] R, Swanepole, J. Phys. E: Sci. Instrum. 17 (1984) 896; https://doi.org/10.1088/0022-

3735/17/10/023
[33] N. El-Kadry, M. F. Ahmed, K. Abdel-Hady, Thin Solid Films, 274 (1996) 120; https://doi.org/10.1016/0040-6090(95)07096-6
[34] M.A. Abdel-Rahim, M.M. Hafiz, M. M. El-Nahass, A. M. Shamekh. Phys. B 387 (2007) 383; https://doi.org/10.1016/j.physb.2006.04.038
[35] F. Urbach. Phys. Rev. 92 (1953) 1324; https://doi.org/10.1103/PhysRev.92.1324
[36] MF. Kotkata, MS. Al-Kotb, FA. Abdel-Wahab, Chalcog. Lett. 7 (2010) 145.
[37] A.H. Ammar, A.M. Farid, M.A.M. Seyam, Vacuum 66 (2002) 27; https://doi.org/10.1016/S0042-207X(01)00417-1
[38] Wemple, S.H. and DiDomenico J., M. Phys. Rev. B, 3 (1971) 1338; https://doi.org/10.1103/PhysRevB.3.1338
[39] M. M. Malik, M. Zulfequar, A. Kumar, M. Husain. J. of Phys. Condensed Mat. 4(43) (1992) 8331; https://doi.org/10.1088/0953-8984/4/43/008
[40] V. D. Das, and Mallik, R.C. Mats. Research Bulletin, 37 (2002) 1961; https://doi.org/10.1016/S0025-5408(02)00810-3
[41] L. Leontic, I. Druta, R. Danac, Synthetic Metals 165 (2006) 224.
[42] M. M. Hafiz, A. H. Moharram, A. A. Abu-Sehly, Appl. Surf. Sci. 252 (1998) 207; https://doi.org/10.1016/S0921-4526(98)00053-2